Polarization volume grating with high efficiency and large diffraction angle

YISHI WENG,[1,2] **DAMING XU,**[1] **YUNING ZHANG,**[2] **XIAOHUA LI,**[2] **AND SHIN-TSON WU**[1,*]

[1]*College of Optics and Photonics, University of Central Florida, Orlando, Florida 32816, USA*
[2]*School of Electronic Science and Engineering, Southeast University, Nanjing 210018, China*
[*]*swu@ucf.edu*

Abstract: We propose a polarization volume grating (PVG), which exhibits nearly 100% diffraction efficiency and large diffraction angle. Both reflective and transmissive PVGs can be configured depending on application preference. Such a PVG is polarization-sensitive so that it can split an incident unpolarized beam into two well-separated yet polarized beams. These outstanding features make PVG a strong candidate for photonic and display applications. To investigate and optimize the diffraction properties, we build a rigorous simulation model based on finite element method. To illustrate its potential applications, we propose a simple 2D/3D wearable display using a planar waveguide comprising of two reflective PVGs.

Reference and links

1. M. G. Moharam, E. B. Grann, D. A. Pommet, and T. K. Gaylord, "Formulation for stable and efficient implementation of the rigorous coupled-wave analysis of binary gratings," J. Opt. Soc. Am. A **12**(5), 1068–1076 (1995).
2. M. G. Moharam and T. K. Gaylord, "Coupled-wave analysis of reflection gratings," Appl. Opt. **20**(2), 240–244 (1981).
3. M. G. Moharam, D. A. Pommet, E. B. Grann, and T. K. Gaylord, "Stable implementation of the rigorous coupled-wave analysis for surface-relief gratings - enhanced transmittance matrix approach," J. Opt. Soc. Am. A **12**(5), 1077–1086 (1995).
4. S. R. Nersisyan, N. V. Tabiryan, D. M. Steeves, and B. R. Kimball, "The promise of diffractive waveplates," Opt. Photonics News **21**(3), 40–45 (2010).
5. S. R. Nersisyan, N. V. Tabiryan, D. M. Steeves, and B. R. Kimball, "The principles of laser beam control with polarization gratings introduced as diffractive waveplates," Proc. SPIE **7775**, 77750U (2010).
6. S. R. Nersisyan, N. V. Tabiryan, D. M. Steeves, and B. R. Kimball, "Characterization of optically imprinted polarization gratings," Appl. Opt. **48**(21), 4062–4067 (2009).
7. C. Oh and M. J. Escuti, "Numerical analysis of polarization gratings using the finite-difference time-domain method," Phys. Rev. A **76**(4), 043815 (2007).
8. P. F. McManamon, P. J. Bos, M. J. Escuti, J. Heikenfeld, S. Serati, H. Xie, and E. A. Watson, "A review of phased array steering for narrow-band electro-optical systems," Proc. IEEE **97**(6), 1078–1096 (2009).
9. Y. Li, J. Kim, and M. Escuti, "Broadband orbital angular momentum manipulation using liquid crystal thin films," Proc. SPIE **8274**, 1–8 (2012).
10. H. Chen, Y. Weng, D. Xu, N. V. Tabiryan, and S.-T. Wu, "Beam steering for virtual/augmented reality displays with a cycloidal diffractive waveplate," Opt. Express **24**(7), 7287–7298 (2016).
11. C. Oh and M. J. Escuti, "Achromatic diffraction from polarization gratings with high efficiency," Opt. Lett. **33**(20), 2287–2289 (2008).
12. R. K. Komanduri, K. F. Lawler, and M. J. Escuti, "Multi-twist retarders: broadband retardation control using self-aligning reactive liquid crystal layers," Opt. Express **21**(1), 404–420 (2013).
13. J. Kobashi, H. Yoshida, and M. Ozaki, "Planar optics with patterned chiral liquid crystals," Nat. Photonics **10**(6), 389–392 (2016).
14. Q. Hong, T. X. Wu, and S. T. Wu, "Optical wave propagation in a cholesteric liquid crystal using the finite element method," Liq. Cryst. **30**(3), 367–375 (2003).
15. T. Todorov, L. Nikolova, and N. Tomova, "Polarization holography. 2: Polarization holographic gratings in photoanisotropic materials with and without intrinsic birefringence," Appl. Opt. **23**(24), 4588–4591 (1984).
16. D. J. Broer, J. Lub, and G. N. Mol, "Wide-band reflective polarizers from cholesteric polymer networks with a pitch gradient," Nature **378**(6556), 467–469 (1995).

17. D. Katsis, D. U. Kim, H. P. Chen, L. J. Rothberg, S. H. Chen, and T. Tsutsui, "Circularly polarized photoluminescence from gradient-pitch chiral-nematic films," Chem. Mater. **13**(2), 643–647 (2001).
18. C. L. Ting, T. H. Lin, C. C. Liao, and A. Y. G. Fuh, "Optical simulation of cholesteric liquid crystal displays using the finite-difference time-domain method," Opt. Express **14**(12), 5594–5606 (2006).
19. D. Kasyanyuk, K. Slyusarenko, J. West, M. Vasnetsov, and Y. Reznikov, "Formation of liquid-crystal cholesteric pitch in the centimeter range," Phys. Rev. E Stat. Nonlin. Soft Matter Phys. **89**(2), 022503 (2014).
20. H. Mukawa, K. Akutsu, I. Matsumura, S. Nakano, T. Yoshida, M. Kuwahara, and K. Aiki, "A full-color eyewear display using planar waveguides with reflection volume holograms," J. Soc. Inf. Disp. **17**(3), 185–193 (2009).
21. Y. Amitai, S. Reinhorn, and A. A. Friesem, "Visor-display design based on planar holographic optics," Appl. Opt. **34**(8), 1352–1356 (1995).
22. J. Han, J. Liu, X. Yao, and Y. Wang, "Portable waveguide display system with a large field of view by integrating freeform elements and volume holograms," Opt. Express **23**(3), 3534–3549 (2015).

1. Introduction

Holographic volume grating (HVG) has been widely used as a diffractive element for beam steering [1–3]. Such a volume grating is formed based on the interference pattern in a hologram recording material, e.g. photopolymer. The most distinctive feature of HVG is when it is illuminated by a Bragg-matched beam, a highly efficient single-order diffraction can be generated and the diffraction angle is quite large. Meanwhile, HVG exhibits a high transmittance because the narrow diffraction bandwidth and high angular selectivity. Another optical element known as diffractive waveplate (DW) [4–6] (also called as polarization grating (PG) or optical axis grating (OAG) [7–9]) has also been demonstrated several years ago. Such a grating exhibits periodic spatial variations along the orientation of optical axis in an anisotropic medium. If the optical axis on a substrate surface rotates periodically along one direction, the structure is called cycloidal diffractive waveplate (CDW). When the thickness of a CDW satisfies what a half-wave plate demands, it can present as a transmission grating. Compared to HVG, the unique feature of CDW is its sensitivity to the input polarization; e.g. a high efficiency + 1st or −1st diffraction order can be obtained depending on the handedness of the incident circularly polarized light. However, the diffraction angle of a CDW is relatively small (~15° in air) and it is difficult to enlarge because of the physical mechanism involved [7, 10]. Such a diffraction angle is much smaller than that an HVG can achieve. Oh, *et al*. [11, 12] proposed an improved CDW scheme for achieving achromatic diffraction. The improved scheme consists of two stacked antisymmetric chiral circular DWs with opposite twist senses, and achromatic diffraction can be achieved by compensating the chromatic dispersion of retardation through the reversed twist structures.

Such a method is enlightening. Compared to a typical CDW, the direction perpendicular to the surface is not homogenous any more. By adding a chiral dopant to a nematic host, the LC would exhibit helical structure and provide another periodicity perpendicular to the surface, which in turn generates a periodically slanted refractive index planes. When the number of periodic refractive index planes is adequate, Bragg diffraction can be established. Same as cholesteric liquid crystal (CLC), this scheme is sensitive to the handedness of circular polarization but can steer the reflected beam without tilting the helical axis. As a result, a Polarization Volume Grating (PVG) is generated. Such a grating offers combined advantages of HVG and CDW, i.e. high diffraction efficiency, large diffraction angle, and polarization selectivity. Recently, to prove concept Kobashi *et al*. [13] demonstrated this scheme by fabricating a reflective patterned CLC with a diffraction angle of 0.453° in the air. In principle, a much larger diffraction angle can be obtained. Similar to HVG, both reflective and transmissive PVGs can be formed.

In this paper, we describe the operation principles of PVGs in detail and build a rigorous simulation model based on finite element method (FEM) to analyze the characteristics of both reflective and transmissive PVGs with commercial software COMSOL. Some unique features of PVG are discussed.

1. Physical principles

In a conventional CLC, a chiral dopant is added to induce helical twist along the vertical direction whereas the LC is homogeneous in the horizontal plane. By contrast, in PVG we introduce another periodic structure in the horizontal plane, as illustrated in Fig. 1. The top substrate is treated to provide a rotation of LC optical axis in xz-plane, and the rotating angle changes continuously and periodically along x-axis with a period of Λ_x. Beneath the top substrate, the LC (or more broadly speaking, birefringent material because a reactive mesogen can also be employed) exhibits helical structure with a period length of Λ_y (or one half of the pitch length p) along y-axis. Such a scheme generates a series of slanted and periodical refractive index planes with slanted angle $\varphi = \pm \arctan (\Lambda_y/ \Lambda_x)$. To simplify the analysis without losing its generality, here we assume $0° < \varphi < 90°$.
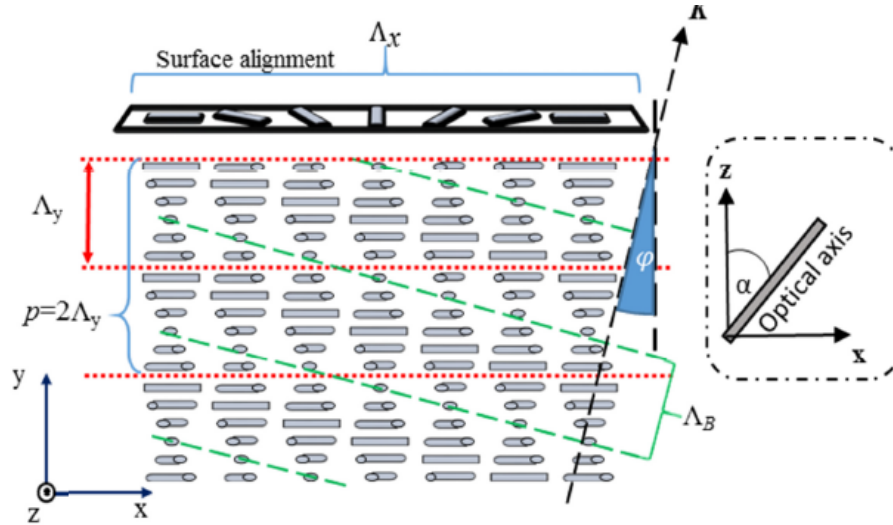

Fig. 1. A schematic diagram of the proposed PVG. The optical axis rotates in xz-plane; the rotating angle α changes continuously and periodically along x and y directions with periods of Λ_x and Λ_y, respectively. The refractive index distribution presents as a tilted volume grating with a tilt angle φ. Bragg diffraction can be established when the medium is thick enough to generate sufficient periodical refractive index planes.

In order to form the periodic surface alignment pattern, various methods can be employed, such as using photopolymers to record the interference patterns of a left- and right-handed circularly polarized beams. The helical structure along y direction can also be easily achieved by doping a chiral dopant into the birefringent host, and the periodicity Λ_y (or pitch length $p = 2\Lambda_y$) can be adjusted via controlling the helical twist power (HTP) and concentration of a chiral dopant. Since the Bragg reflection requires several periods to establish, the birefringent material needs to be thick enough to allow several pitches in the bulk.

Due to the helical twisting power of chiral dopant, the LC directors (optical axis) would rotate along the helix. Unlike conventional CLC, due to the periodic surface alignment pattern, the LC directors at different positions would rotate with different azimuthal angle in xz-plane. However, if we observe the LC directors along an oblique direction, the LC optical axis with same azimuthal angles are actually aligned at a tilted angle, as shown by the green dashed lines in Fig. 1. The azimuthal angles of optical axis rotation α with different coordinates in a PVG are determined by following equation:

$$\alpha = \frac{\pi}{\Lambda_x} x + \frac{\pi}{\Lambda_y} y, \tag{1}$$

wherein the period length Λ_x and Λ_y correspond to the optical axis rotation of π due to the equivalence between the optical rotations of $m\pi$ (m = 0, 1, 2, 3......) for a birefringent material. When the LC layer is thick enough, Bragg diffraction can be established. As a result, the normally incident light would be diffracted and the Bragg diffraction is governed by:

$$2n_{eff}\Lambda_B \cos\varphi = \lambda_B. \tag{2}$$

In Eq. (2), λ_B is the Bragg wavelength in vacuum, Λ_B is the Bragg period and φ is the slanted angle of periodical refractive index planes or represented as the slanted angle of the grating vector $\boldsymbol{K}$ (see Fig. 1), and n_{eff} is the effective refractive index of the birefringent medium defined by [14]:

$$n_{eff} = \sqrt{(n_e^2 + 2n_o^2)/3}. \tag{3}$$

The Bragg period Λ_B has simple geometric relationships with Λ_x and Λ_y as:

$$\begin{cases} \Lambda_x = \Lambda_B / \sin\varphi \\ \Lambda_y = \Lambda_B / \cos\varphi \end{cases}. \tag{4}$$

Generally speaking, both reflective and transmissive PVGs can be fabricated, depending on the direction of the incident and diffracted beams. For a reflective grating, the diffracted beam is on the same side as the incident beam as depicted in Fig. 2(a), while for a transmissive grating the incident and diffracted beams are on the different sides as shown in Fig. 2(b). When the incident angle $\theta_i = 0°$, the PVG can be distinguished between the reflective and transmissive types simply by the range of slanted angle φ. Based on the theory of volume grating [1], the relationship between slanted angle φ and the first-order diffraction angle θ_{diff} when $\theta_i = 0°$ is given by:

$$\theta_{diff} = \begin{cases} 2\varphi & 0 \le \varphi < \dfrac{\pi}{4} \\ \pi - 2\varphi & \dfrac{\pi}{4} < \varphi < \dfrac{\pi}{2} \end{cases}. \tag{5}$$

In Eq. (5), when $0 < \varphi < \pi/4$ the PVG works as a reflective grating, while $\pi/4 < \varphi < \pi/2$ it functions as a transmissive grating.
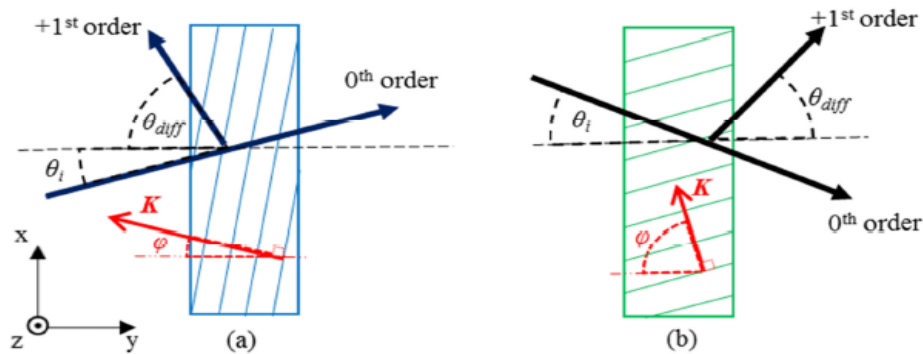

Fig. 2. Geometry and notation of diffraction orders for (a) reflective PVG and (b) transmissive PVG: θ_i is the incident angle and θ_{diff} is the diffraction angle for the first-order. The 0th order is the transmitted beam without diffraction.

To fabricate the surface alignment with periodically rotated optical axis, a possible method is to expose the reactive mesogen using a beam with constant intensity but spatially varying polarization. Kobashi *et al.* [13] utilized an LCD projector and rotatable waveplate to sequentially project light beams with different linear polarization angles. In this method, an *x*-direction periodicity of 80 μm was achieved, but the diffraction angle is only 0.453° due to the large period.

To increase diffraction angle, a much smaller periodicity along *x*-axis is required. A feasible approach is to use a photo-alignment material to record the interference pattern of two orthogonal circularly polarized beams so that the structure shown in Fig. 3 can be fabricated [15]. The periodicity can be adjusted by changing the angle between the two exposure beams. Compared to mechanical scanning or rotating techniques, the holographic exposure process is much faster and more precise Although same holographic exposure setup using two orthogonal circularly polarized beams has been used for fabricating the CDWs with smaller periodicity [4, 5], the largest diffraction angle is still limited because the physical mechanism involved is a planar phase grating. In contrast, our PVG performs as a volume grating through adding another periodicity perpendicular to the surface, which can generate a much larger diffraction angle based on Bragg diffraction.
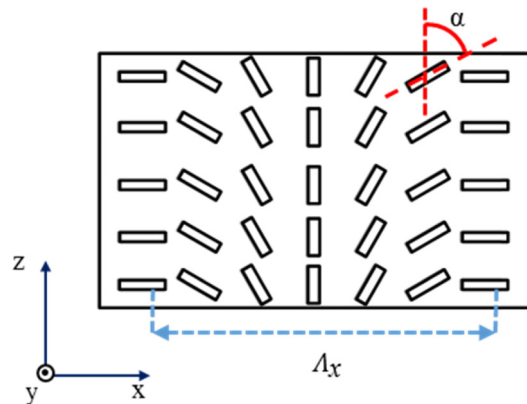

Fig. 3. The surface alignment pattern. It is an interference pattern generated by two orthogonal circularly polarized beams, which can be recorded in a photoalignment material after exposure.

Figure 4 depicts the polarization states of diffraction order for the reflective and transmissive PVGs. Both PVGs can diffract the circularly polarized incident light which has the same handedness as the helix twist in PVGs (left-handed in Fig. 4). For the reflective PVG, the polarization of the first order keeps the same handedness as that of the incident beam. For the transmissive PVG, the handedness in the first-order is converted to an orthogonal direction, which is similar to that of CDW. When the incident beam has an orthogonal handedness to the helical twist of the PVG (right-handed), it will transmit to the 0th order without changing the polarization.
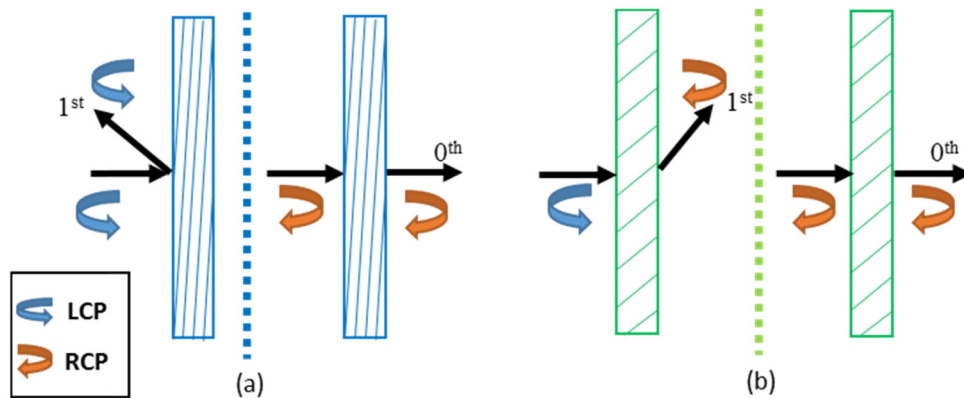
Fig. 4. Schematic diagram of the polarization states of diffraction order for (a) reflective and (b) transmissive PVGs when the normally incident beam is left-handed circular polarization (LCP) and right-handed circular polarization (RCP), respectively. The handedness of the helical twist in both reflective and transmissive PVGs are assumed to be left-handed along the incident direction.

In next section, a rigorous computational model based on Finite Element Method (FEM) is built to simulate and analyze the properties of the reflective and transmissive PVGs, respectively.

2. Modeling of PVG

To investigate the diffractive properties of PVG, we have built a rigorous model based on FEM using the COMSOL Multiphysics, which is a commercial finite element package.
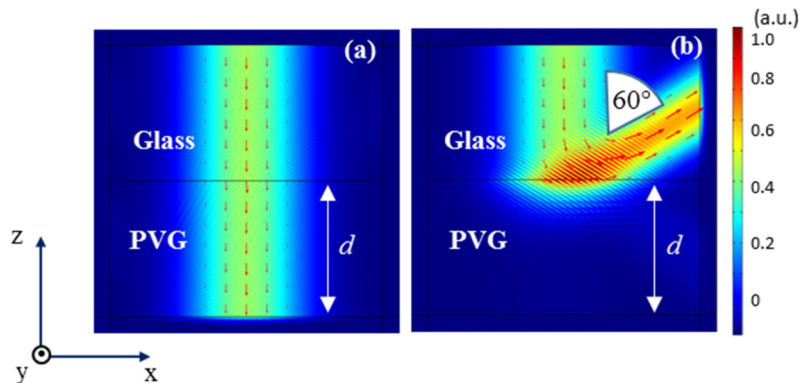
3.1 Reflective PVG

Fig. 5. The simulated electric field distribution with different circularly polarized incident beam using COMSOL Multiphysics: (a) Left-handed circularly polarized light, and (b) right-handed circularly polarized light. Bragg reflection occurs when the incident beam has same handedness as the twist helix in the reflective PVG (right-handed in simulation). In simulation, we assume birefringence $\Delta n = 0.2$ ($n_e = 1.7$, $n_o = 1.5$), PVG thickness $d = 4$ μm, refractive index of glass $n_{glass} = 1.57$ and operation wavelength $\lambda = 550$ nm. Red arrows represent the power flow or Poynting vector.

The simulated results of a reflective PVG illuminated by a left-handed or a right-handed circularly polarized beam at normal incidence are shown in Figs. 5(a) and 5(b), respectively. In simulation, the period length along x and y directions are set as $\Lambda_x = 404.6$ nm and $\Lambda_y = 233.6$ nm, which corresponds to the slanted angle $\varphi = 30°$ in PVG. The twist helix in the PVG is right-handed and the diffraction with high efficiency can be generated when the incident

circularly polarized beam has the same handedness, as shown in Fig. 5(b). In Fig. 5(b) the diffraction angle is 60° in glass ($n = 1.57$) as an illustrated example. In fact, an arbitrary diffraction angle can be obtained by adjusting the period length Λ_x or Λ_y along x and y directions, as outlined below.

Figure 6(a) shows the diffraction efficiency spectra at different diffraction angles. From Fig. 6(a), the diffraction efficiency and bandwidth are almost independent of the diffraction angles. This is a very favorable feature, as the PVG can diffract light to different angles with high diffraction efficiency and constant bandwidth. The angular response for different diffraction angles is also depicted in Fig. 6(b). It shows that the angular bandwidth become narrower with a larger diffractive angle. In fact, the angular bandwidth of PVGs is much wider than that of HVGs, which would benefit many applications such as enlarging the field of view for near-eye display applications.
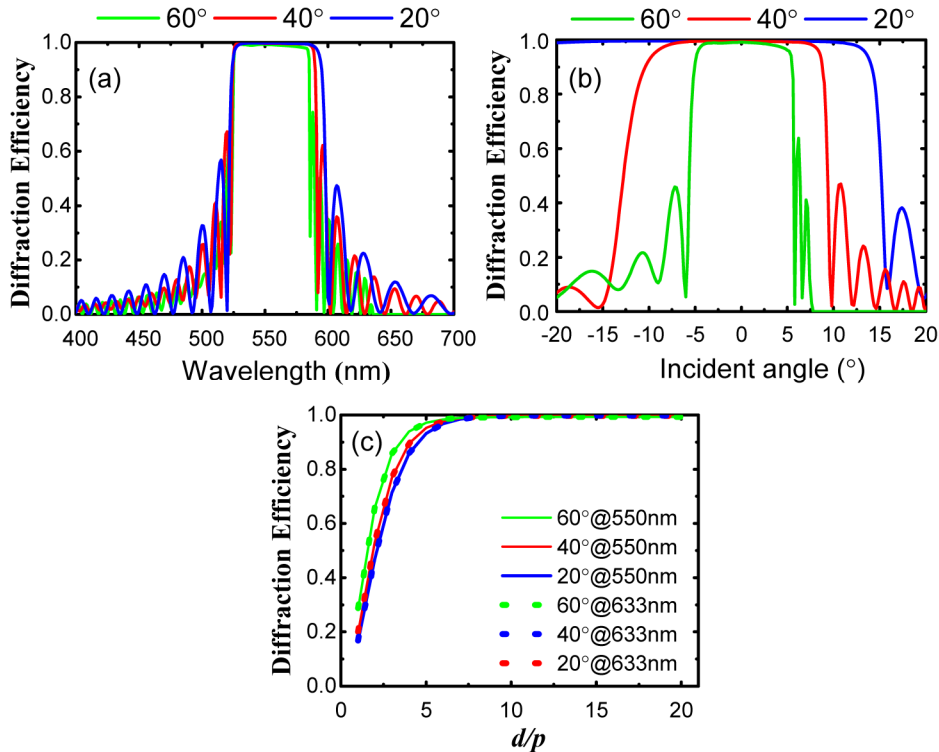

Fig. 6. Diffraction behavior of a reflective PVG for different diffraction angles in glass ($n = 1.57$): (a) diffraction efficiency spectra with normal incidence (0°) and (b) angular response with incident wavelength $\lambda = 550$nm. In (a) and (b) we assume the Bragg wavelength $\lambda_B = 550$ nm at normal incidence (0°) (c) Diffraction efficiency as a function of d/p for different operation wavelengths. When $d/p > 7$, diffraction efficiency over 98% can be achieved. The corresponding thickness required for the three specified diffraction angles (20°, 40°, 60° in glass ($n = 1.57$)) is 2.52 μm, 2.8 μm and 3.29 μm when $\lambda = 550$ nm, and 2.94 μm, 3.19 μm and 3.73 μm when $\lambda = 633$ nm. In simulation, we assume $\Delta n = 0.2$ ($n_e = 1.7$, $n_o = 1.5$), and the incident beam has same handedness as the twist helix in the reflective PVG.

On the other hand, cell gap plays an important role affecting the electro-optic performance of PVGs. To establish Bragg diffraction, the cell gap should be thick enough as we mentioned before. Figure 6(c) depicts the thickness requirement for a reflective PVG at different diffraction angles. Because the pitch length varies as the diffraction angle and Bragg wavelength change, here we characterize the thickness properties using d/p, which parameterizes the number of helical pitches in the LC layer. As Fig. 6(c) shows, the diffraction efficiency is insensitive to the operation wavelength λ. Therefore, for a certain

diffraction angle, the required thickness for achieving high diffraction efficiency can be easily obtained based on the number of pitches. When the value of d/p is over 7, diffraction efficiency higher than 98% can be achieved for all conditions in Fig. 6(c). The corresponding thickness required for the three diffraction angles (20°, 40°, 60° in glass ($n = 1.57$)) is 2.52 μm, 2.8 μm and 3.29 μm at $\lambda = 550$ nm, and 2.94 μm, 3.19 μm and 3.73 μm when $\lambda = 633$ nm. Compared to a conventional volume holographic grating whose thickness is at least tens of micrometers, the thickness of our PVG is much thinner.

The electro-optic performance of PVGs also depends on the birefringence of the employed LC. Figure 7(a) depicts the efficiency spectra with different Δn. High birefringence material helps broaden the diffraction bandwidth, same as the spectral properties of CLC. The relationship between the Δn and angular selectivity is also studied and shown in Fig. 7(b). The trend is clear: as Δn increases, the angular band of incident light for achieving high diffraction efficiency becomes broader. This is highly desirable in many applications, such as head-mounted displays. Compared to the refractive index modulation in a HVG, which is usually in the order of 10^{-2}, the LC birefringence is much higher (e.g. $\Delta n = 0.2$ is pretty common). As a result, the PVG has advantages in both diffraction spectra and angular bandwidth over conventional HVG. Moreover, due to the polarization selectivity of PVGs, high transmission can be achieved for an unpolarized incident beam, which is another important feature for some applications.
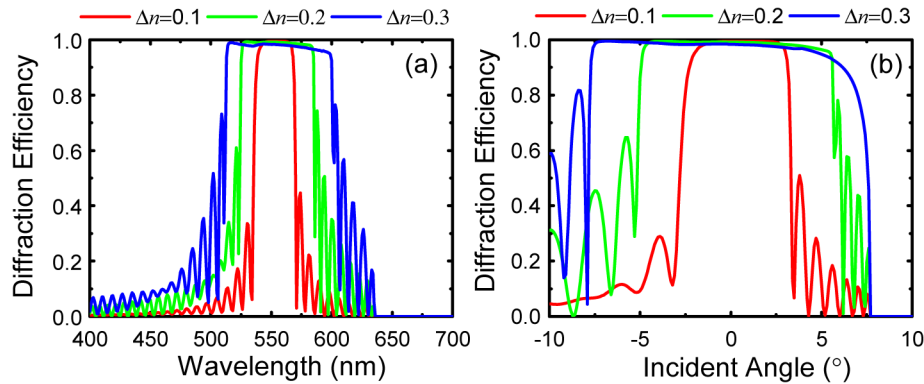

Fig. 7. The effects of Δn on a reflective PVG: (a) Diffraction efficiency spectra and (b) diffraction efficiency with different incident angles. In simulation, $n_o = 1.5$, $d = 4$ μm and the diffraction angle is 60° at $\lambda = 550$ nm.

In a CLC, the bandwidth of Bragg reflection can be broadened using a gradient pitch length [14], and the approaches for realizing the gradient pitch profile have been reported in [16, 17]. This strategy can also be applied to reflective PVG, in which a gradient pitch is generated along y direction while the periodicity along x direction is fixed. The twist angle of the optical axis with gradient pitch length is defined by [18]:

$$\alpha_{gradient} = \frac{\pi}{\Lambda_x}x + \frac{\pi}{\Lambda_{y0}}y + (\frac{\pi}{\Lambda_{y1}} - \frac{\pi}{\Lambda_{y0}})\frac{y^2}{2d},$$ (6)

where Λ_x is the period length along x axis, d is the cell gap, Λ_{y0} and Λ_{y1} are the period lengths along y axis near the top surface and bottom surface, respectively. Because the period lengths Λ_{y0} and Λ_{y1} correspond to the optical axis rotation of π while the pitch length p corresponds to 2π rotation, the gradient pitch lengths represented in Eq. (6) range from $2\Lambda_{y0}$ to $2\Lambda_{y1}$ within the cell gap. The diffraction efficiency spectra for the gradient pitch and uniform pitch are depicted in Fig. 8. It is clear that gradient pitch helps broaden the reflection band for a reflective PVG. As the gradient pitch covers a wider range, the reflection band becomes broader (red line).
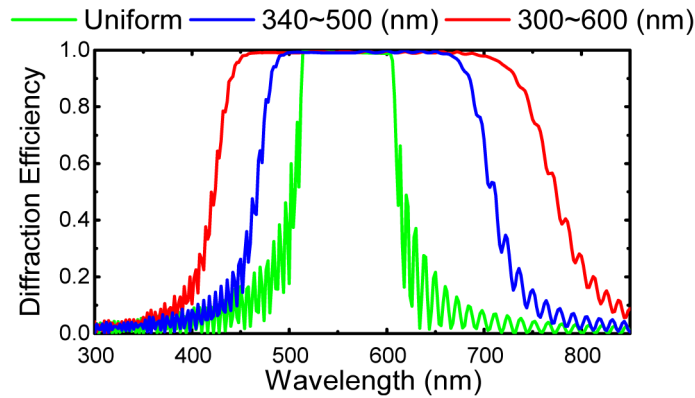
Fig. 8. Simulated diffraction efficiency spectra of the reflective PVGs with uniform pitch and gradient pitch. For gradient pitch, two specific pitch range ($p = 340\sim500$ nm and $p = 300\sim600$ nm) are simulated. In simulation, we assumed birefringence $\Delta n = 0.3$, $n_o = 1.5$, and the thickness of reflective PVG is $d = 8$ μm.

3.2 Transmissive PVG

Transmissive diffractive optical elements have been widely used in beam steering and displays. For example, a CDW can diffract light to the ± 1st orders based on the handedness of incident circularly polarized light with high diffraction efficiency (>98%). This feature renders CDW very attractive for the eye-tracking of a virtual reality display. However, the diffraction efficiency decreases dramatically when the diffraction angle (in air) exceeds 15°. Our transmission-type PVGs can achieve a much better performance in this aspect. Figures 9(a) and 9(b) compare the diffraction far-field intensity patterns between a CDW and a transmissive PVG. A typical CDW diffracts right- and left-handed circularly polarized incident beams into two orders (± 1st) respectively with 15° diffraction angle in air. In contrast, for the transmissive PVG, a high efficiency diffraction (+ 1st or −1st order) occurs only when the circularly polarized incidence has the same handedness as the optical axis rotation in the PVG, and the orthogonal handedness part is transmitted (0th order). Compared to CDW, the transmissive PVG exhibits a larger diffraction angle (45° in air).
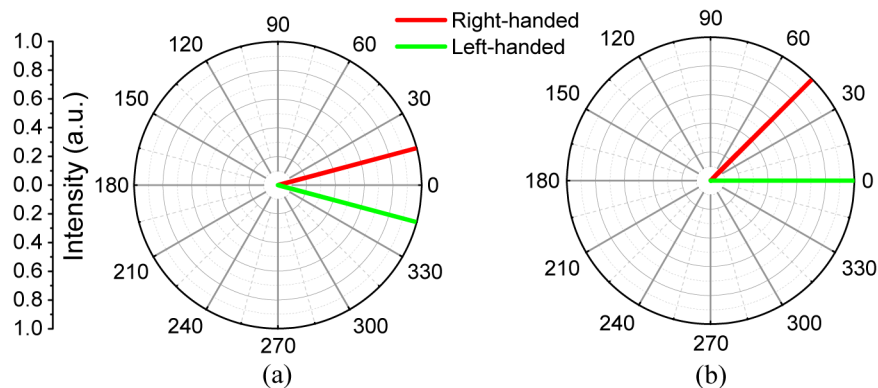

Fig. 9. Simulated far-field diffraction pattern for (a) CDW and (b) transmissive PVG. Two orthogonal circularly polarized beams at normal incidence (0°) were set as the incident light, respectively.

It is noteworthy that the Fresnel reflection at the air-PVG interface becomes stronger as the diffraction angle increases. For large diffraction angles, an anti-reflection coating can be used to enhance the diffraction efficiency by reducing the reflection at the air-PVG interface.

To investigate the diffractive properties of our PVG without the effect from the Fresnel reflections, we set a Perfectly Matched Layer (PML, which is an artificial absorbing layer) instead of the air layer in our simulation model and the diffraction angle in air is calculated by Snell's law.

As mentioned above, in order to establish Bragg diffraction for the reflective PVGs, a sufficient number of helical pitches is required. However, for a transmissive PVG, the periodical accumulation for Bragg diffraction is provided mainly along x direction due to $45° < \varphi < 90°$. As a result, the thickness of transmissive PVG is thinner than that of the reflective type.
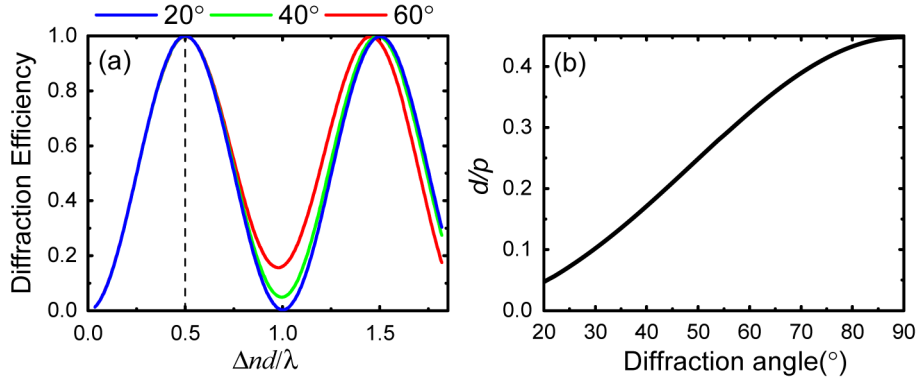

Fig. 10. (a) Relation between −1st order diffraction efficiency and thickness for a transmissive PVG with different diffraction angles in air. $\Delta n = 0.2$. A right-handed circularly polarized light with $\lambda = 550$ nm was used as input. (b) The pitch length (or period length along y direction) requirement for different diffraction angles as $d = 1.37$ μm.

The thickness requirement of transmissive PVG for different diffraction angles are shown in Fig. 10(a). Here, the incident light is a circularly polarized light with the same handedness as the optical axis rotation in PVG ($\lambda = 550$ nm, $\Delta n = 0.2$). From Fig. 10(a), we find that the first maximum diffraction efficiency of the −1st order appears at $d\Delta n/\lambda \approx 0.5$, i.e. $d \approx 1.37$ μm for all three specified diffraction angles. Therefore, a large transmission diffraction angle can be generated by adding a small amount of chiral dopants to a typical CDW without changing the thickness. The period length along x and y directions should be adjusted for the desired diffraction angle. When $d \approx \lambda/(2\Delta n)$, the relation between the values of d/p and diffraction angles is depicted in Fig. 10(b). We note that a longer pitch length p is required when the diffraction angle is small [19]. Meanwhile, considering the unique properties of transmissive PVGs, most of application scenarios should utilize it as a large diffraction angle grating with high efficiency where the pitch length is in a common range.

To obtain more comprehensive understanding on the properties of a transmissive PVG, we simulate its diffraction spectra and angular response. Results are plotted in Figs. 11(a) and 11(b). It shows that high diffraction efficiency (~100%) can be obtained when the Bragg condition is matched ($\lambda = 550$ nm and incident angle $\theta_i = 0°$). For a larger diffraction angle, say 60° (blue lines), both the wavelength and angular bandwidth become narrower.
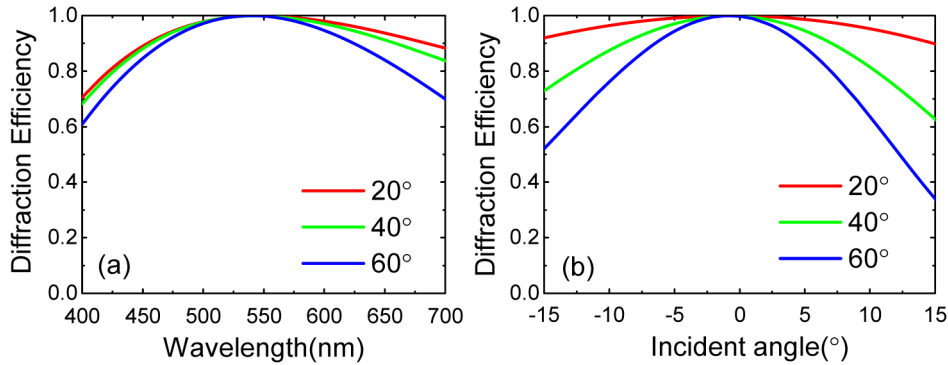
Fig. 11. Diffraction behavior of a transmissive PVG for different diffraction angles in air: (a) diffraction efficiency spectra and (b) angular response for the −1st order. In simulation, the input circularly polarized light has the same handedness as the optical axis rotation in PVG. The Bragg wavelength for all diffraction angles is 550 nm and LC Δn is 0.2.

In comparison with reflective PVG, the diffraction performance of a transmissive PVG is less sensitive to the birefringence. The diffraction spectra and angular sensitivity for different Δn are shown in Fig. 12. It shows that the wavelength band is also insensitive to Δn. On the other hand, as Δn increases the angular band becomes broader. Therefore, a high Δn material is favored when a wide range of incident angle is required.

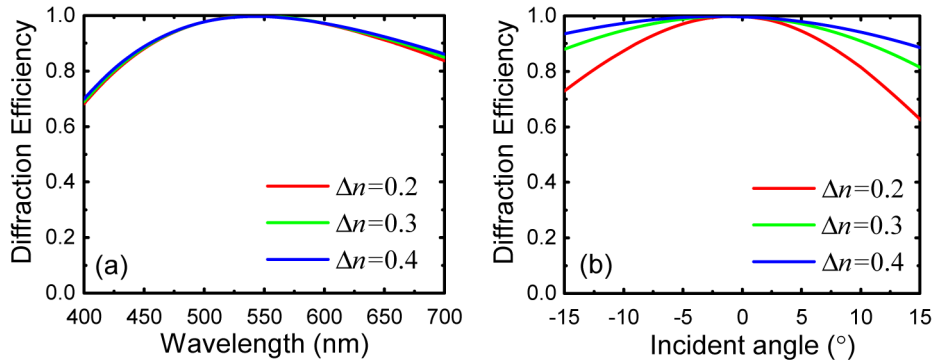Fig. 12. Δn effect of a transmissive PVG: (a) simulated diffraction efficiency spectra and (b) diffraction efficiency with different incident angles. In simulations, we assume $n_o = 1.5$, $d = \lambda_B /(2\Delta n)$, and $\lambda_B = 550$ nm.

In abovementioned simulations, the circularly polarized incidence is assumed to have the same handedness as the optical axis rotation of the birefringent medium. Next, we discuss the diffraction behavior of a transmissive PVG when the incident light has orthogonal handedness to the optical axis rotation. The CDW diffracts two orthogonal circularly polarized incident beams into + 1st and −1st orders respectively. In contrast, the transmissive PVG only diffracts the incident light that has same handedness as the chiral dopant and transmits another orthogonal handedness without diffraction (0th order). Thus, there is a significant difference between the CDW and the transmissive PVG. However, the difference gradually disappears as diffraction angle decreases. As discussed earlier, when the diffraction angle decreases, the period length along y direction grows (see Fig. 10(b)). An extreme case is when the diffraction angle is 0°, the period length along y direction will be infinity. In this case, no periodicity exists along y direction and the transmissive PVG degenerates to a typical CDW.
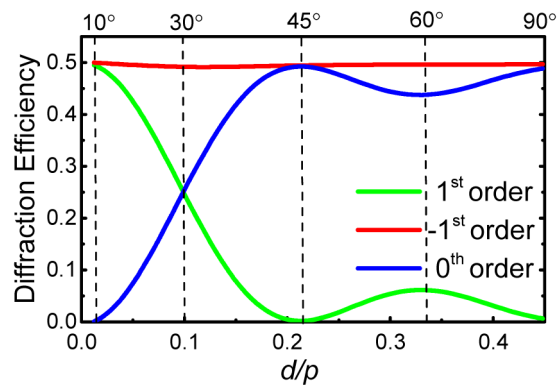
Fig. 13. Simulated diffraction efficiency for different orders as a function of *d/p*. The input is a linearly polarized plane wave with λ = 550 nm. The birefringence Δn is 0.2 and thickness $d = \lambda/(2\Delta n)$ = 1.37 μm. The values in top indicate the corresponding diffraction angles of the 1st order in air for some specific *d/p* ratios.

We investigate the process of degeneration by using a linearly polarized incident light, which can be decomposed into two orthogonal circularly polarized beams. With the variation of *d/p*, the diffraction efficiency for the different orders is depicted in Fig. 13. In simulation, we assumed the thickness $d = \lambda/(2\Delta n)$, and the simulation results indicate that only three diffraction orders (0, ± 1) are nonzero (>0.01%). In Fig. 13, the diffraction efficiency of the −1st order is independent of *d/p* (or diffraction angle) and its diffraction efficiency keeps at ~50%, which corresponds to the diffraction for the half of the incident light having the same handedness as the optical axis in the PVG (right-handed in Fig. 13). For the remaining half (left-handed), the diffraction efficiency is partitioned between −1st and 0th orders, depending on the *d/p* value. When *d/p*≈0, the pitch length is near to infinity and the periodicity along y direction disappears, as a result, the transmissive PVG degenerates into a typical CDW that diffracts the two orthogonal circularly polarized incident light into + 1st and −1st orders, respectively. With increased *d/p*, diffraction efficiency in + 1st decreases rapidly and leaks into the 0th order. The diffraction efficiency of 0th order reaches a maximum (~50%) when *d/p*≈0.2 (or diffraction angle ≈45° in air), which means all the left-handed circularly polarized beams transmit as the 0th order without diffraction. For *d/p* >0.2, the diffraction efficiency experiences a slight fluctuation between the + 1st and 0th orders as *d/p* keep increasing, but the diffraction efficiency in 0th order remains at a high level and the unique property of PVG is maintained. The results depicted in Fig. 13 are instructive and the appropriate range of *d/p* should be adjusted based on the application requirement.

3. Potential applications

Due to the outstanding properties, the PVG can be used in various devices for beam steering, optical switching, and displays. Specifically, a 2D/3D wearable display using planar waveguides with the reflective PVGs is proposed here as an example of potential applications.

Wearable display with planar waveguide design using HVGs has been developed for years [20–22]. To realize its 3D capability, a traditional HVG-based wearable display usually requires two display panels to provide different images to the left and right eyes of the viewer. As mentioned before, compared to HVG our PVG is distinguished by the feature of polarization sensitivity. By replacing the HVGs with PVGs, the 3D capability can be obtained for a waveguide-designed wearable display with only one microdisplay, which not only greatly simplifies the device structure but also reduces the weight and cost of the display.

The schematic diagram is shown in Fig. 14, in which two reflective PVGs doped with right- and left-handed chiral dopants are stacked as an in-coupled gratings. The PVGs diffract

right- and left-handed circularly polarized incident beams respectively and transmit another orthogonal circularly polarized beams. Since the handedness of chiral dopants is orthogonal in two PVGs, the diffractive angles for the two PVGs are $+2\varphi$ and -2φ for normal incidence based on Eq. (5), and as long as the diffractive angle is larger than the Total Internal Reflection (TIR) angle (θ_{TIR}) in the waveguide, the image from the microdisplay would be guided in the waveguide. Figure 15 shows the simulation results for the in-coupled stacked-PVGs. In a wearable (or head-mounted) display, two reflective PVGs are placed in front of left and right eyes with a mirror symmetrically positioned as the out-coupled gratings. The two out-coupled gratings diffract the propagating image separately, and break the TIR condition that finally sends the output beam to each eye, respectively. With the help of polarization switchable display, different images can be sent to left and right eyes respectively and sequentially, which can realize 3D images in a waveguide-designed wearable display with only one display panel. Meanwhile, such a device can also work in a 2D mode as long as sending the same image to the left and right eyes. As a result, a simple 2D/3D wearable display can be obtained.
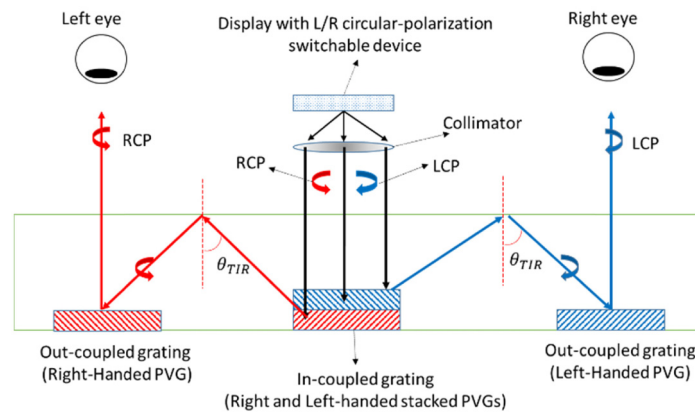

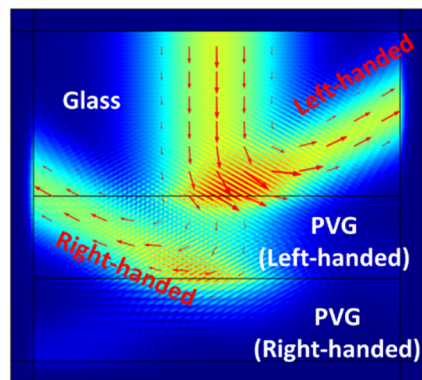Fig. 14. Schematic diagram of a 2D/3D wearable display using planar waveguides with the reflective PVGs.

Fig. 15. Simulated results for the stacked two PVGs used as an in-coupled grating in a wearable display device. A linear polarized incident beam was split into two orthogonal circular polarized beam with two diffracted angles. In simulation, we assume birefringence $\Delta n = 0.2$ ($n_e = 1.7$, $n_o = 1.5$), each PVG thickness is 4 μm, refractive index of glass $n_{glass} = 1.57$ and operation wavelength $\lambda = 550$ nm. Red arrows represent the power flow or Poynting vector.

4. Conclusion

We show the design and performance of a new diffractive element called Polarization Volume Grating (PVG). We describe its operation principles in detail, and demonstrate that such a PVG can be configured in reflective or transmissive type, depending on the application preferences. To investigate its diffraction behaviors, we built a rigorous simulation model using finite element method. The fundamentally diffractive properties including diffraction efficiency, operation bandwidth, angular response and sensitivity of polarization are presented for both reflective and transmissive PVGs. This work represents the first numerical analysis for such a unique optical element, and the simulated results validate that both reflective and transmissive PVGs with a few microns thickness can generate nearly 100% diffraction efficiency and large diffraction angle with a specific incident polarization. These distinctive features make the PVG attractive for photonic and display applications. As an example of potential applications, a new 2D/3D wearable display using planar waveguides with two reflective PVGs is proposed, which provides 3D capability to a simple waveguide-based wearable display.